applied sciences

MDPI

Article

4-Methoxy Sulfonyl Paeonol Inhibits Hepatic Stellate Cell Activation and Liver Fibrosis by Blocking the TGF-β1/Smad, PDGF-BB/MAPK and Akt Signaling Pathways

Yi-Jen Liao [1,†], Yuan-Hsi Wang [1,†], Chao-Lien Liu [1], Cheng-Chieh Fang [1], Ming-Hua Hsu [2,*] and Fat-Moon Suk [3,4,*]

1 School of Medical Laboratory Science and Biotechnology, College of Medical Science and Technology, Taipei Medical University, Taipei 110, Taiwan; yjliao@tmu.edu.tw (Y.-J.L.); m609105001@tmu.edu.tw (Y.-H.W.); chaolien@tmu.edu.tw (C.-L.L.); kingbike1201@gmail.com (C.-C.F.)

2 Department of Chemistry, National Changhua University of Education, Chuanghua 50007, Taiwan

3 Division of Gastroenterology, Department of Internal Medicine, Wan Fang Hospital, Taipei Medical University, Taipei 116, Taiwan

4 Department of Internal Medicine, School of Medicine, College of Medicine, Taipei Medical University, Taipei 110, Taiwan

* Correspondence: minghuahsu@cc.ncue.edu.tw (M.-H.H.); 95351@w.tmu.edu.tw (F.-M.S.); Tel: +886-4-7232105 (ext. 3511) (M.-H.H.); +886-2-27328232 (F.-M.S.)

† Equal contribution.

Received: 17 July 2020; Accepted: 25 August 2020; Published: 27 August 2020

Abstract: Liver fibrosis initiates the progression of cirrhosis, and, finally, hepatocellular carcinoma (HCC). The increased proliferation and activation of hepatic stellate cells (HSCs) are crucial for hepatic fibrogenesis. Paeonol is the major vigorous component of Cortex Moutan, a traditional herbal medicine widely used for treating various diseases. Here, we identified a novel paeonol derivative (4-methoxy sulfonyl paeonol, 4-MSP) that inhibits TGF-β1-induced Smad2/3 phosphorylation and collagen expression in HSCs. 4-MSP pretreatment suppressed the PDGF-BB–induced phosphorylation of MAPK pathway members (MEK/ERK, p38, JNK), Akt/p70S6K, and HSC proliferation. However, 4-MSP treatment had no effect on the induction of apoptosis in HSCs. The microarray experiments showed that 4-MSP treatment affects the TGF-β signaling, MAPK cascade, and other pathways related to HSCs activation and proliferation. The administration of 4-MSP to a liver fibrosis mouse model induced by CCl_4 significantly decreased the expression of hepatic fibrosis markers (α-SMA, col1A2, TGF-β, and MMP2), and attenuated hepatic collagen deposition and liver damage. In addition, no adverse effects were observed in 4-MSP exposed mice. In conclusion, this novel paeonol-phenylsulfonyl derivative prevents the progression of liver fibrosis through blocking TGF-β1/Smad, PDGF-BB/MAPK, and Akt signaling, which suggests its use as a novel therapeutic against liver fibrosis.

Keywords: hepatic stellate cells (HSCs); liver fibrosis; paeonol derivative

1. Introduction

Many etiologies lead to the formation of liver fibrosis, including viral hepatitis (HCV or/and HBV), nonalcoholic fatty liver disease, abuse in ethyl alcohol consumption (alcoholic steatohepatitis), and nonalcoholic steatohepatitis [1–3]. Once liver fibrosis proceeds, the normal liver architecture would be disrupted, and the normal organ function would change and eventually lead to a massive amount of scarring and organ failure, resulting in cirrhosis and hepatocellular carcinoma (HCC) [1–3]. Since most

of the primary liver malignancies were developed with a background of fibrotic or cirrhotic, to explore effective therapeutic methods to alleviate liver fibrosis is urgently needed. Hepatic fibrosis corresponds to the proliferation of myofibroblasts, excessive amplification, and abnormal deposition of extracellular matrix (ECM) [4]. When a liver is injured, the activated hepatic stellate cells (HSCs), that produce a lot of ECM in the liver, are recognized as major cells in the progression of liver fibrosis [5]. In a normal liver, HSCs maintain a quiescent phenotype, and are mainly discovered in the perisinusoidal space, with the function of vitamin A storage [6]. While in liver injury, they transdifferentiate from the quiescent state into activated myofibroblast phenotypes that are proliferative, contractile, inflammatory, and chemotactic [7–10]. Therefore, a novel compound that possesses the ability to deactivate the HSCs is important for liver fibrosis treatment. Transforming growth factor-β1 (TGF-β1), a key cytokine, is involved in the formation of liver fibrosis. TGF-β1 directly induces collagen 1 and α-smooth muscle actin (α-SMA) expressed in HSCs through a phosphorylation of downstream Smad2/3 proteins [11–13]. TGF-β1 also enhances the ECM proteins synthesis and restrains their degradation [14]. Blocking the TGF-β1 signaling transduction obviously inhibits liver fibrosis [15,16]. In terms of TGF-β1, platelet-derived growth factor-BB (PDGF-BB) and VEGF released from activating HSCs are important factors for sustaining activation and proliferation of HSCs [7]. Previous studies had found that dysregulated PDGF-BB signaling pathway is the major inducement for the HSCs trans-differentiation, and also an important pathological factor for liver fibrosis [17]. PDGF-BB activates Ras, subsequently propagating stimulatory signaling via phosphorylation of the MAPK and Akt signaling pathways [11]. Blockade of PDGF signaling reduced experimental liver fibrogenesis [17]. The inhibition of TGF-β1 and blockade of Akt/P70S6K axis, as well as ERK signaling, have been proven to alleviate HSC activation [18,19].

Natural plants have been used as the major source of food and medicine worldwide for thousands of years. Chinese herbs are an abundant resource, and have promising application prospects for treating different diseases. Paeonol (a phenolic) is the main active element of Cortex Moutan, which is used in traditional Chinese herbal medicine. Ample pharmacological evidence suggests that paeonol has a lot of biological functions, including antioxidant, anti-inflammatory, antitumor, antidiabetic, anti-cardiovascular disease, and neuroprotective effects [20,21]. Paeonol enhanced the apoptosis of ovarian tumor cells by decreasing surviving expression and initiating activity of caspase 3 [22]. Paeonol also had a radio-enhancing effect on lung adenocarcinoma [23] and attenuated acute lung injury in lipopolysaccharide-induced shock rats [24]. Additionally, paeonol has shown anti-alcoholic fatty liver [25] and anti-liver cancer [26] activities. Because of the pharmacological and physiological significances of paeonol for treatment of different diseases, some paeonol derivatives have been synthesized, and these compounds have considerable drug discovery potential in medicinal chemistry [21]. The introduction of a phenylsulfonyl moiety into a compound was found to improve the solubility of the compound and enhance its biological activity [27,28]. Previously, we designed a series of paeonol-phenylsulfonyl derivatives and found that 4-methoxy sulfonyl paeonol (4-MSP) (Figure 1a) significantly inhibits HBV gene expression and viral DNA replication [29]. However, the antifibrotic effects of 4-MSP in the liver are still unknown. In this study, we showed that 4-MSP exerts antifibrotic effects by suppressing TGF-β1/Smad, PDGF-BB/MAPK, and Akt signaling, both in cells and in the mouse model.

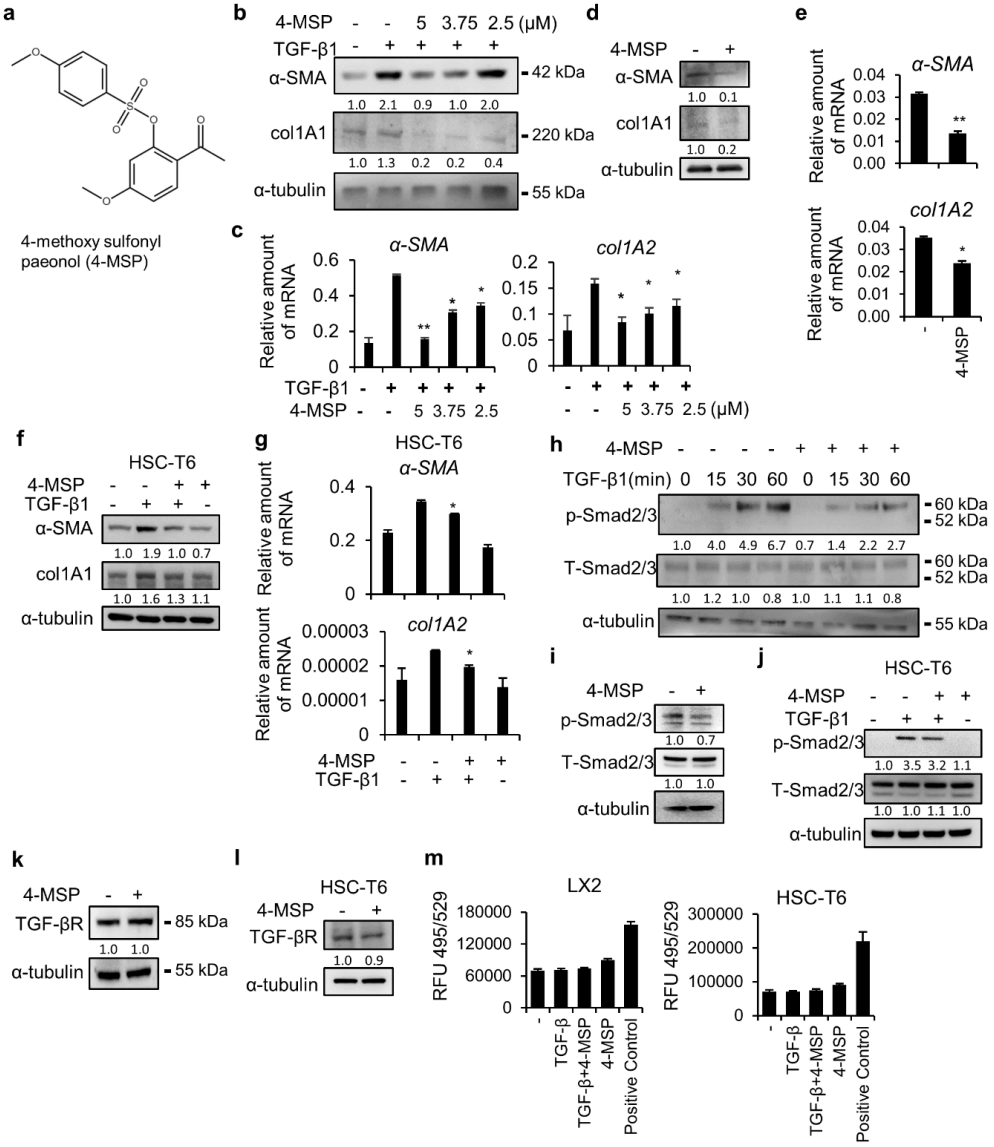

Figure 1. Compound 4-MSP inhibits TGF-β1-induced hepatic stellate cells (HSCs) activation. (**a**) Structure of 4-methoxy sulfonyl paeonol (4-MSP). (**b**) LX2 cells were treated with TGF-β1 (10 ng/mL) and 4-MSP for 24 h. Western blot analyzed the protein levels of α-SMA, col1A1, and α-tubulin. (**c**) Real-time PCR detected mRNA levels of α-SMA and col1A2 relative to that of GAPDH. *: $p < 0.05$ vs. TGF-β1 alone group; **: $p < 0.01$ vs. TGF-β1 alone group. (**d**) LX2 cells were treated with 4-MSP for 24 h. Western blot analyzed the protein levels of α-SMA, col1A1, and α-tubulin. (**e**) Real-time RT-PCR detected mRNA levels of α-SMA and col1A2 relative to that of GAPDH. *: $p < 0.05$ vs. control group; **: $p < 0.01$ vs. control group. (**f**) HSC-T6 cells were treated with TGF-β1 (10 ng/mL) and 4-MSP for 24 h. Western blot analyzed the protein levels of α-SMA, col1A1, and α-tubulin. (**g**) Real-time RT-PCR detected mRNA levels of α-SMA and col1A2 relative to that of GAPDH. *: $p < 0.05$ vs. TGF-β1 alone group. (**h**) Pre-treated LX2 cells with 5 μM of 4-MSP overnight and then subjected to TGF-β1 (10 ng/mL) for indicated times. Phosphorylation- and total-Smad2/3 were analyzed by western blot. (**i**) LX2 cells were treated with 4-MSP for 24 h. Phosphorylation- and total-Smad2/3 were analyzed by western blot. (**j**) Pre-treated HSC-T6 cells with 5 μM of 4-MSP overnight and then subjected to TGF-β1 (10 ng/mL) for 30 min. Phosphor- and total-Smad2/3 were analyzed by western blot. (**k**) LX2 cells were treated with 4-MSP for 24 h. Western blot analyzed the protein levels of TGF-βR and α-tubulin. (**l**) HSC-T6 cells were treated with 4-MSP for 24 h. Western blot analyzed the protein levels of TGF-βR and α-tubulin. (**m**) Cellular reactive oxygen species (ROS) levels were performed by using the commercial ROS detection assay kit, according to the manufacturer's instructions. Data are presented for three independent experiments, with similar results.

2. Materials and Methods

2.1. 4-Methoxy Sulfonyl Paeonol (4-MSP)

Figure 1a shows the structure of 4-methoxy sulfonyl paeonol (4-MSP). The detailed synthase of the compound 4-MSP was described in our previous study [29]. Compound 4-MSP was dissolved in solvent DMSO and used in this study at the indicated concentrations.

2.2. Cell Culture

LX2 cells are human HSC cell lines, and HSC-T6 are immortalized strain of rat HSCs. Both cells were obtained from S. Friedman [30]. Cell culture conditions were described previously [31].

2.3. TGF-β1, PDGF-BB, and 4-MSP Treatments

For the effects of 4-MSP on HSC activation, LX2 cells were treated with media supplemented with TGF-β1 or PDGF-BB (R&D Systems, Minneapolis, MN, USA) at 10 ng/mL with, or without, 4-MSP. To determine the effects of 4-MSP on intracellular signaling pathways, LX2 cells were incubated overnight, supplemented with 5 μM 4-MSP, followed by stimulation with 10 ng/mL TGF-β1 or PDGF-BB at different time periods.

2.4. Cytotoxicity Assays

Cell viability was measured using an alamarBlue assay kit (Life Technologies, Carlsbad, CA, USA). Cellular growth was detected according to cellular reaction of the REDOX indicator to change from oxidized form to reduced form. LX2 cells (5×10^3 cells/well) were plated in a 96-well plate for 24 h. Cells were then added to alamarBlue reagent and incubated in a cell incubator for 2.5 h. The absorbance was recorded at 570 nm, while the reference wavelength used was 600 nm. The survival percentages were determined by OD values of the treatment groups correlated to the solvent control group.

2.5. Wound Healing Assays

LX2 cells were seeded in dishes (ibidi GmbH, Martinsried, Germany) and grown overnight. The culture inserts were removed, and were filled with culture medium containing 10 ng/mL PDGF-BB and 5 μM 4-MSP.

2.6. Gene Expression Profiling

To compare relative gene expression profiles, the total mRNA was extracted, purified, and analyzed by a OneArray® Gene Microarrays (Phalanx Biotech, Hsinchu, Taiwan). Briefly, total RNA of LX2 cells cotreated with 5 μM 4-MSP plus 10 ng/mL TGF-β1 for 24 h was extracted for analysis of whole-genome gene expression. Gene expression profiling of these samples was determined by chips of OneArray Plus (Phalanx Biotech Group). Hierarchical clustering of the assays was conducted using Cluster 3.0 software (Stanford University School of Medicine, Stanford, CA, USA), which is available online (http://bonsai.hgc.jp/~{}mdehoon/software/cluster/). A significant change in mRNA expression was defined as a 1.5-fold increase or decrease of the signal intensity. According to results of microassay, Kyoto Encyclopedia of Genes and Genomes (KEGG) pathway analysis and Gene Ontology (GO) term enrichment were used in the connection between key genes and pathways related to HSC activation.

2.7. Animals and Experimental Design

All animal protocols were approved by the Institutional Animal Care and Use Committee of Taipei Medical University (No. LAC-2017-0476). The animals received humane care according to the institutional guidelines and the Animal Research: Reporting of In Vivo Experiments (ARRIVE) guidelines. Male C57BL/6 mice (8 weeks) were obtained from the National Laboratory Animal Center, Taiwan. Mice were housed in plastic cages with standard chow diet, and maintained in twelve

hours light and twelve hours dark conditions. The animals were randomly divided into four groups: (1) vehicle control; (2) CCl_4 (intraperitoneal (i.p.) administration of 2 m/kg body weight (BW) CCl_4 [in corn oil at 1:5 *v*/*v*] two times every week and continued for 6 weeks); (3) 4-MSP + CCl_4 (daily i.p. injection of 5 mg/kg BW 4-MSP for 1 week with concomitant CCl_4 injection for another 6 weeks); and (4) 4-MSP (daily intraperitoneal injection of 5 mg/kg 4-MSP for 6 weeks). 500 mg of compound 4-MSP was prepared in solvent DMSO (1 mL). The 4-MSP was further diluted into the indicated concentrations by using the normal saline (0.1% of DMSO). Obtained serum and liver samples were used for subsequent experiments. The tissues were frozen and stored at −80 °C, while some were prepared using 10% formalin fixed for immunohistochemical (IHC) staining.

2.8. Hydroxyproline Assays

The concentration of hydroxyproline in liver sections were analyzed by using BioVision colorimetric kit (BioVision, Mountain View, CA, USA).

2.9. Western Blotting, IHC Analysis and Blood Biochemical Parameter Measurement

CelLytic lysis buffer containing protease ($NaVO_3$, NaS, and $Na_4P_2O_7$) and phosphatase inhibitors (Leupton, TLCK, TPCK, Aport, and PMSF) was used for lysing liver specimens and cell samples. Western blotting conditions were described previously [31]. Rabbit antibodies against p-Smad2(Ser465/467)/3(Ser423/425), T-Smad2/3, p-ERK(Thr202/Tyr204), T-ERK, p-MEK(Ser217/221), T-MEK, p-AKT(Ser473), T-AKT, p-p38(Thr180/Tyr182), T-p38, p-JNK(Thr183/Tyr185), T-JNK, p-P70S6K(Thr389), T-p70S6K, p-PDGFR(Tyr751), T-PDGFR, TGF-βR, Caspase-3, Caspase-9, and PARP were purchased from Cell Signaling Technology (Beverly, MA, USA). Rabbit anti-α-SMA was purchased from Abcam (Cambridge, MA, USA). Mouse anti-α-tubulin was acquired from Sigma-Aldrich. Hematoxylin and eosin (H&E) staining was obtained for histopathological examination of liver sections. Sirius Red staining (Abcam) and Masson's Trichrome staining (Abcam) of liver sections were conducted, according to the manufacturer's instructions, to qualitatively assess the architecture of collagen and extent of fibrosis. IHC staining of F4/80 (1:200; Cell Signaling, Beverly, MA, USA) was detected by using the EnVision+Dual Link System-HRP (DAB+) kit (DakoCytomation, Carpinteria, CA, USA). Serum levels of alanine aminotransferase (ALT), albumin, and blood urea nitrogen (BUN) were analyzed by a biochemical analyzer (VetTest^{TM}, IDEXX, westbrook, ME, USA).

2.10. Quantitative Real-Time PCR (QPCR)

Total RNA from mouse liver was extracted using TRIzol reagent (Ambion, Carlsbad, CA, USA), according to the manufacturer's standard protocols. Complementary DNA (cDNA) was synthesized by reverse-transcription of two microgram RNA using the High-Capacity cDNA Reverse Transcription Kit with RNase Inhibitor (Thermo Fisher Scientific, Waltham, MA, USA). Each sample was assayed in triplicate by a Light Cycler Real-Time PCR System (Roche diagnostics, Mannheim, Germany). The housekeeping gene GAPDH was used for gene expression studies. The following primers sequences of interested genes used in real-time PCR (Q-PCR) were shown: collagen type 1 alpha 2 (col1A2): 5′-TAGGCCATTGTGTATGCAGC-3′ (F) and 5′- ACATGTTCAGCTTTGTGGACC-3′ (R); α-SMA, 5′-GTTCAGTGGTGCCTCTGTCA-3′ (F), and 5′-ACTGGGACGACATGGAAAAG-3′ (R); MMP2, 5′-CTCAGATCCGTGGTGAGAT-3′ (F), and 5′-AGGCTGGTCAGTGGCTTGG-3′ (R); TGF-β1: 5′-CGAAGCGGACTACTATGC-3′ (F) and 5′-GTTGCTCCACACTTGATTT-3′ (R); Bcl-xl, 5′-GCTGCATTGTTCCCGTAGAG-3′ (F), and 5′-GTTGGATGGCCACCTATCTG-3′ (R); Bax, 5′-TGCTTCAGGGTTTCATCCAG-3′ (F), and 5′-GGCGGCAATCATCCTCTG-3′ (R); TNF-α, 5′-TGTAGCCCATGTTGTAGCAAACC-3′ (F), and 5′-GAGGACCTGGGAGTAGATGAGGTA-3′ (R); F4/80, 5′-CAAGACTGACAACCAGACG-3′ (F), and 5′-ACAGAAGCAGAGATTATGACC-3′ (R); PDGF-BB: 5′-GTCGAGTTGGAAAGCTCATCTC-3′ (F) and 5′-GAGATGAGCTTTCCAACTCGAC-3′ (R); GAPDH: 5′-TCACCACCATGGAGAAGGC-3′ (F) and 5′-GCTAAGCAGTTGGTGGTGCA-3′ (R).

2.11. Statistical Analyses

Data are expressed as the means ± standard deviations (SDs) of three independent experiments. SPSS v.13.0 software (v. 13.0, SPSS Inc. Chicago, IL, USA) was used for statistical analyses. A two-tailed Student's t-test was used for inter-group comparisons, with a difference of $p < 0.05$ indicating a statistical significance.

3. Results

3.1. Compound 4-MSP Inhibits TGF-β1-Induced HSC Activation

From the previous report, we know that activated HSCs are responsible for liver fibrosis, due to the deposition of excessive ECM and increased collagen accumulation mediated by TGF-β1 [11,13]. Therefore, we first determined whether 4-MSP suppresses the HSC activation through inhibiting the TGF-β1 signaling pathway. First, we performed the western blot to analyze the expressed levels of α-SMA and collagen 1A1 (col1A1). Results revealed that TGF-β1-induced α-SMA and col1A1 upregulation were decreased in 4-MSP-treated LX2 cells, especially under the dosage of 5 μM (Figure 1b). The QPCR analysis was also conducted to investigate mRNA levels of α-SMA and clo1A2. Results showed that 4-MSP treatment reduced the expression levels of α-SMA and clo1A2 in a dose-dependent manner (Figure 1c). In addition, we also found that cells treated with 4-MSP alongside also inhibited the protein and mRNA expression levels of α-SMA and collagen 1 (Figure 1d,e). Moreover, we used the rat hepatic stellate cell line, HSC-T6, to further confirm the result found in LX2 cells. Similarly, the 4-MSP treatment inhibited the TGF-β1-induced protein and mRNA expression levels of α-SMA and collagen 1 in HSC-T6 cells (Figure 1f,g), while 4-MSP alongside treatment had no effect on changing the expression levels of α-SMA and collagen 1 in HSC-T6 cells (Figure 1f,g). TGF-β1 signaling pathway activation is triggered by TGF-β1 interacting with its receptor. The Smad protein is then phosphorylated, and subsequently triggers a production of collagen [8,11]. Thence, we further investigated whether 4-MSP treatment inhibits Smad pathway activation in TGF-β1-treated HSCs. In Figure 1h, 4-MSP treatment reduced the phosphorylation of Smad2 (60 kDa), relative to that of the control. We also found that 4-MSP alongside treatment reduced the Smad2 phosphorylation (Figure 1i). In HSC-T6 cells, 4-MSP treatment also inhibited the TGF-β1-induced phosphorylation of Smad2 (Figure 1j). To further elucidate whether the 4-MSP influenced the expression levels of TGF-β receptor (TGF-βR), the western blot experiment was performed. The results showed that treatment of 4-MSP had no effect on changing the protein expression levels of TGF-βR in both LX2 and HSC-T6 cells (Figure 1k,l). We also measured the intracellular levels of reactive oxygen species (ROS) in two HSC's cell lines. The results showed that treatment of either TGF-β or 4-MSP did not affect the levels of ROS in both LX2 and HSC-T6 cells (Figure 1m). These results indicate that compound 4-MSP inhibits TGF-β1-induced activation of HSC through direct inhibition of Smad2/3 phosphorylation and α-SMA/col1A2 expression.

3.2. Compound 4-MSP Inhibits HSC Proliferation Through Blocking PDGF-BB-Induced MAPK and Akt Signalings

Since the initiation of HSC proliferation is a critical stage in promoting liver fibrogenesis [7], we next evaluate the anti-proliferation effects of 4-MSP on HSCs. LX2 cells were treated with 0~20 μM 4-MSP for 24–96 h, and the results showed that dose-dependent and time-dependent inhibition of LX2 cell proliferation was observed after 4-MSP treatment (Figure 2a). It had been reported that PDGF-BB is the main stimulus for HSCs proliferation [11]; we further examined the change of the activation of MAPK and AKT signaling pathway after 4-MSP treatment in LX2 cells. The results indicated that 4-MSP pretreatment decreased the PDGF-BB-mediated phosphorylation of MEK/ERK, JNK, and p38 (Figure 2b). Moreover, Akt and p70S6K phosphorylation showed a decrease in the 4-MSP pretreated cells, compared with that of the control (Figure 2c). These phenomena were also found in the HSC-T6 cells. Treatment of 4-MSP significantly inhibited the PDGF-BB-mediated phosphorylation

of MEK/ERK, JNK, Akt, and p70S6K (Figure 2d,e). To further elucidate whether the 4-MSP affected the expression levels of PDGF receptor (PDGFR) or influenced the phosphorylation of PDGFR, the western blot experiment was performed. The results demonstrated that treatment of 4-MSP did not affect the phosphorylation of PDGFR or the total expression levels of PDGFR in two HSCs cell lines (Figure 2f,g). Furthermore, we also performed the wound healing assay to analyze the effect of 4-MSP on the cell migration ability. The results showed that treatment of 4-MSP inhibited the PDGF-induced cell migration ability in LX2 cells (Figure 2h).

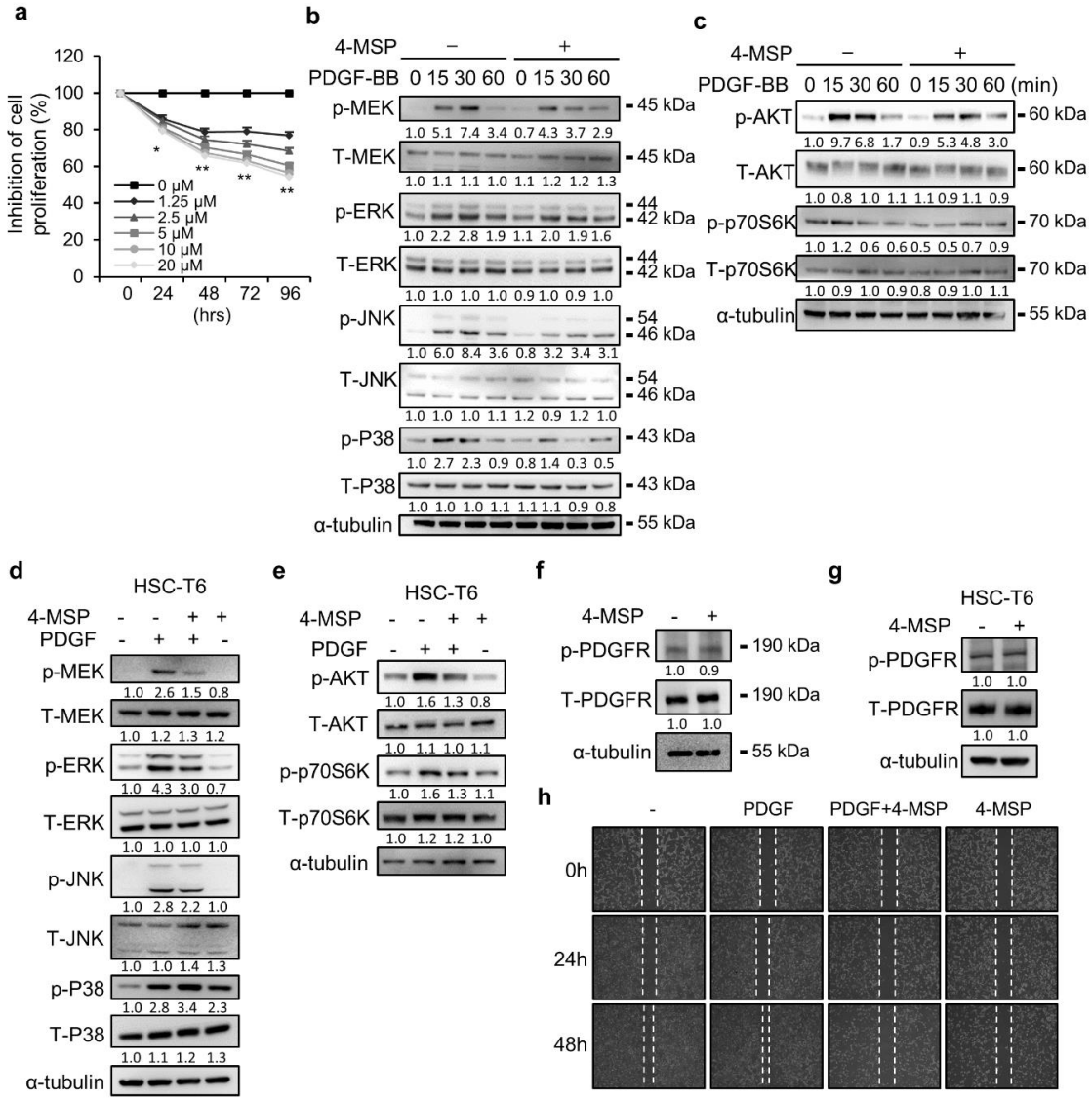

Figure 2. Compound 4-MSP inhibits HSCs proliferation via inhibiting MAPK and AKT signaling pathways. (**a**) LX2 cells in the treatment of 4-MSP at 1.25~20 μM for indicated times, and then subjected to alamarBlue analysis. (**b**,**c**) Pre-treated LX2 cells with 5 μM of 4-MSP overnight, and then subjected to PDGF-BB (10 ng/mL) for indicated times. Phosphorylation and total indicated proteins were analyzed by western blot. (**d**,**e**) Pre-treated HSC-T6 cells with 5 μM of 4-MSP overnight, and then subjected to PDGF-BB (10 ng/mL) for 30 min. Phosphorylation and total indicated proteins were analyzed by western blot. (**f**,**g**) LX2 and HSC-T6 cells were treated with 5 μM of 4-MSP for 24 h. Western blot analyzed the protein levels of p-PDGFR, T-PDGFR, and α-tubulin. (**h**) LX2 cells were treated with PDGF-BB (10 ng/mL) and 4-MSP for indicated times. The cell migration was documented by using a digital camera. Data are presented for at least three independent experiments, with similar results.

3.3. Compound 4-MSP Treatment Does Not Induce Apoptosis in HSCs

Next, we examined whether 4-MSP inhibits cell growth through promoting the apoptosis signaling pathway. The doxorubicin or staurosporine were used as a positive control (PC) in the experiments. As shown in Figure 3a, 4-MSP treatment did not affect caspase-3, PARP, and caspase-9 cleavage. The mRNA levels of Bcl-xl and Bax were not different between 4-MSP-treated and -untreated cells (Figure 3b). Similarly, treatment of 4-MSP did not influence the cleavage of caspase-3, PARP, and caspase-9 (Figure 3c) and the mRNA expression levels of Bcl-xl and Bax (Figure 3d) in HSC-T6 cells. These results reveal that the mechanisms of 4-MSP-mediated inhibition of LX2 and HSC-T6 cell activation arose mainly from the inhibition of cell proliferation via the MAPK and AKT pathways, rather than induction of the apoptotic pathway.

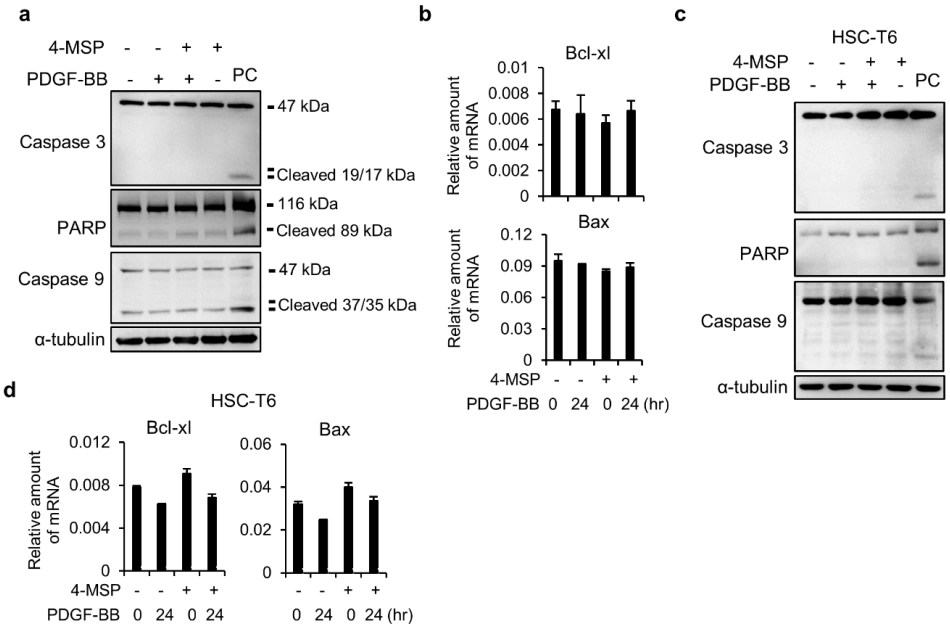

Figure 3. Compound 4-MSP treatment did not induce apoptosis in HSCs. Treatment of LX2 and HSC-T6 cells with PDGF-BB (10 ng/mL) and 4-MSP (5 μM) for 24 h. (**a**,**c**) Protein levels of Caspase-9, PARP cleavage, and α-tubulin were analyzed by western blotting. PC: positive control. (**b**,**d**) mRNA levels of Bcl-xl and Bax, relative to that of GAPDH, were measured by real-time RT-PCR. Data shown are at least three independent experiments with similar results.

3.4. The Effects of Genes and Biological Functions Caused by 4-MSP-Treated HSCs

To examine the alterations of gene expression profile after TGF-β1 and 4-MSP treatment, the microarray experiments were performed. In microarray analysis, the signal intensity with a 1.5-fold increase or decrease was defined as significantly altered in mRNA expression (Figure 4a). To narrow down genes that were affected after 4-MSP treatment, a Venn diagram was performed. The result showed that 74 genes that were downregulated and 92 genes that were upregulated after TGF-β1 treatment were reversed after being treated with 4-MSP (Figure 4b,c). These genes (166 genes) were further used to investigate the pathways changed by 4-MSP treatment. In KEGG pathway enrichment analysis, we found that 4-MSP affected the pathways related to NOD-like receptor signaling, transcriptional misregulation in cancer, TGF-beta signaling, and NF-kappa B signaling pathways (Figure 4d). GO term enrichment results showed that inflammatory response, negative regulation of cell proliferation, MAPK cascade, and signal transduction were affected with the 4-MSP treatment (Figure 4e). These results imply the possibility that 4-MSP treatment influences HSCs activation and proliferation.

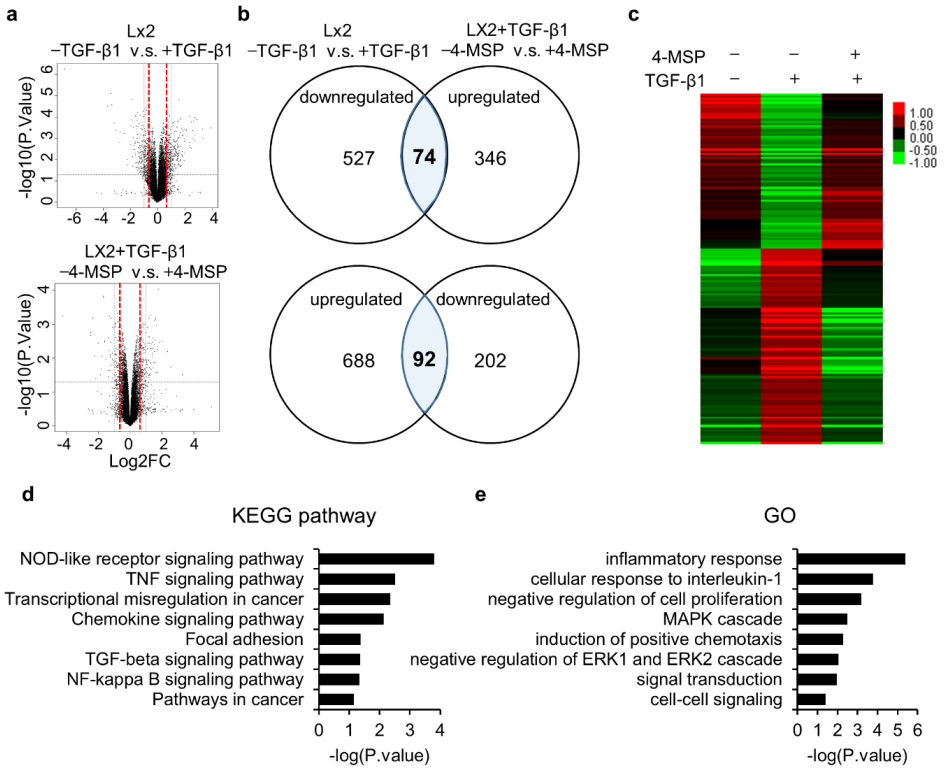

Figure 4. Gene expression profile of TGF-β1 and 4-MSP-treated LX2 cells. (**a**) The volcano plot shows the distribution of differentially expressed genes according to 1.5-fold change (red axis). (**b**) The Venn diagrams show the correlations for up- and downregulated genes between LX2 ± TGF-β1 and LX2+ TGF-β1 ± 4-MSP. (**c**) The heat map of 166 4-MSP-affected genes, based on mRNA microarray analysis. Red and green represent the increase and the decrease in the gene expression levels, respectively. (**d**,**e**) Kyoto Encyclopedia of Genes and Genomes (KEGG) pathway and Gene Ontology (GO) term enrichment analysis for 166 4-MSP-affected genes.

3.5. Compound 4-MSP Ameliorates Fibrosis Process in Mice With CCl_4-Induced Liver Fibrosis Without Inducing Adverse Effects

To further examine the antifibrotic efficacy of 4-MSP, we used the intraperitoneal injection of CCl_4, a widely-used experimental mouse model of liver fibrosis, in the experiments. In Figure 5a, 4-MSP treatment inhibited the CCl_4-induced upregulation of hepatic α-SMA expression. Besides this, the protein expression levels of phosphor-PDGFR and TGF-βR remained unchanged in four groups. Surprisingly, we found that CCl_4 administration induced upregulation of PDGFR, and treatment of 4-MSP significantly reversed the effects (Figure 5a). The QPCR results showed that treatment of 4-MSP inhibited the expression of α-SMA, col1A2, TGF-β, and MMP2 in the liver (Figure 5b). Besides this, the PDGF-BB mRNA levels were also measured. Figure 5b shows that 4-MSP treatment did not change the PDGF-BB expression. H&E staining was used for hepatic pathological examination, and the results demonstrated that CCl_4 induced significantly irregular infiltration borders, perinuclear vacuoles, changes in liver fat, and regional inflammation in the liver, whereas treatment with the 4-MSP demonstrated a normal hepatic morphology (Figure 5c). Collagen deposition was determined by Sirius Red and Masson's Trichrome staining. Results showed that the deposition of collagen was significantly increased in CCl_4-treated mice, whereas this deposition event was reduced in 4-MSP-treated mice (Figure 5c). The results of hydroxyproline assay showed that 4-MSP treatment slightly reduced the CCl_4-induced hydroxyproline accumulation (Figure 1d). To further investigate the effect of 4-MSP in affecting liver inflammation, the TNF-α and F4/80 mRNA expression levels were analyzed. The QPCR results found that treatment of 4-MSP significantly inhibited TNF-α and F4/80 expression (Figure 5b).

Besides this, the F4/80 staining indicated that 4-MSP injection markedly attenuated F4/80 expression, followed by CCl_4 treatment in the liver section (Figure 5c). Moreover, the mouse body weight and serum contents of ALT, albumin, and BUN were not significantly different after 4-MSP treatment (Figure 5e,f). These data indicate that 4-MSP administration attenuated liver fibrosis, as well as liver damage, in mice with CCl_4-induced liver fibrosis, without inducing any overt signs of toxicity in mice.

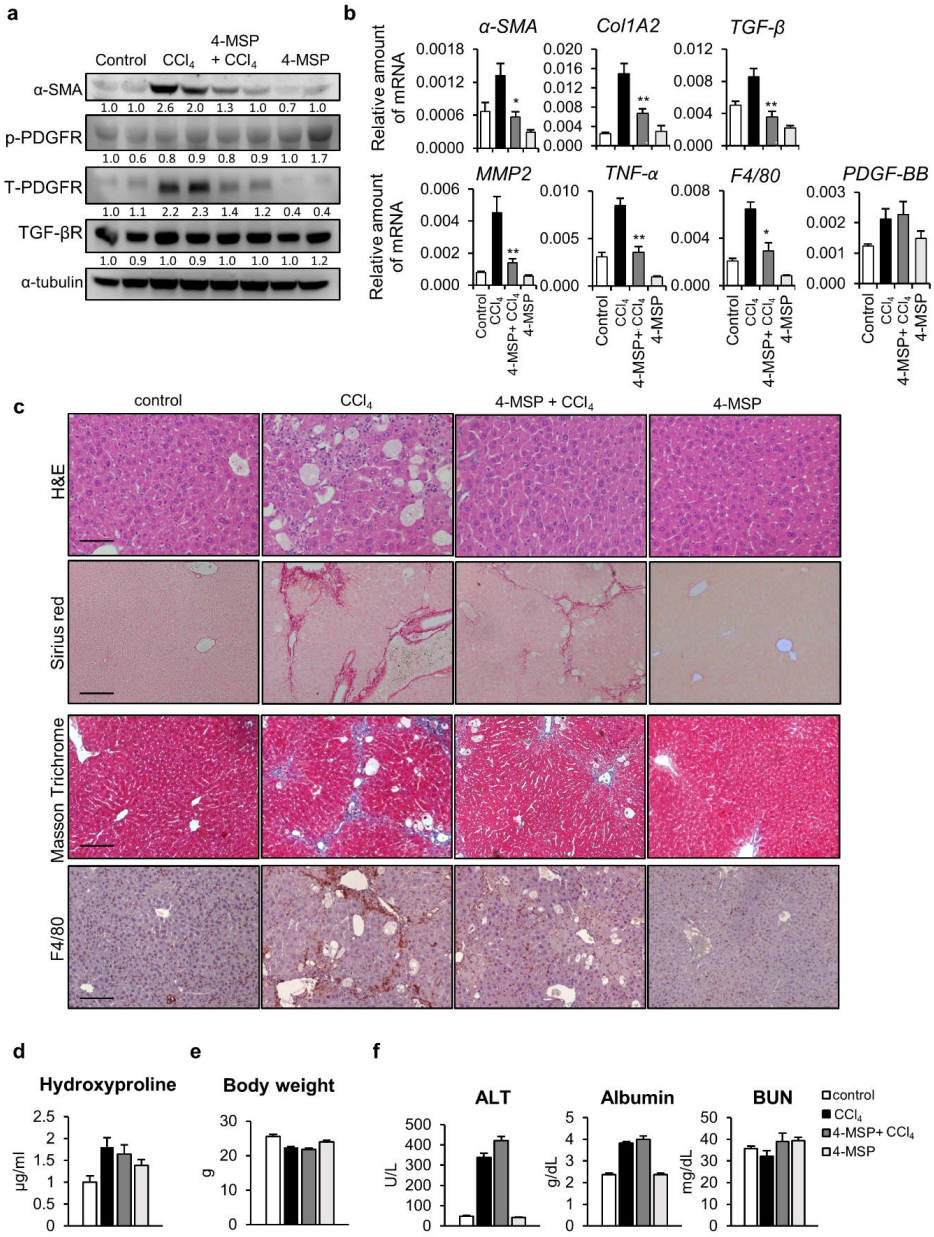

Figure 5. Mice treated with compound 4-MSP attenuate CCl_4-induced liver damage and fibrosis. (**a**) Hepatic protein levels of α-SMA, T/P-PDGFR, TGF-βR, and α-tubulin from four groups were analyzed by western blot. (**b**) mRNA levels of α-SMA, col1A2, TGF-β, MMP2, TNF-α, and F4/80 relative to that of GAPDH (n = 6 per group) were measured by RT-PCR. Data are expressed as the mean ± SD. *: $p < 0.05$ vs. CCl_4 alone group; **: $p < 0.01$ vs. CCl_4 alone group. (**c**) Representative images of H&E, Sirius Red, Masson's Trichrome stainings, and F4/80 immunohistochemical (IHC) staining of liver tissues from each treatment group. The black bar represents a length of 0.1 mm. (**d**) Liver hydroxyproline quantification was performed, according to the manufacturer's instruction. (**e**) Mean body weight of individual mouse group at the endpoint of the experiment. (**f**) Serum samples were acquired at the endpoint of the experiment, and the BUN, albumin, and ALT values were assessed.

4. Discussion

Liver cirrhosis is a serious health issue worldwide which is usually correlated with an economic burden [32]. Furthermore, to prevent the progression of fibrosis that leads to cirrhosis is critical to improving the life quality of patients. When the liver is exposed to dangerous stimulations, normal HSCs are transdifferentiated from the quiescent type into active myofibroblasts that are responsible for the extracellular matrix proteins expression and secretion, including collagen, elastin, proteoglycans, and some of the glycoproteins [33]. The activation of HSCs is considered a key phenomenon in the progression of liver fibrosis; hence, preventing an activation of HSCs is a promising strategy for liver fibrosis treatment. Cortex Moutan, a traditional herbal medicine, is popularly used to treat a lot of diseases worldwide. Paeonol is a phenolic compound and a major active component isolated from Cortex Moutan [21]. Paeonol has been approved by the China FDA, and its pharmacological effects are used to treat various diseases, including tumors, inflammatory diseases, cardiovascular diseases, and neurological diseases [20]. When the treatment of liver cancer with paeonol was examined, paeonol not only decreased oxidative injury and improved immune function in HCC rats [26], but also reversed endoplasmic reticulum stress-induced doxorubicin resistance in HCC [34]. In addition, paeonol treatment was found to alleviate drug- and alcohol-induced acute liver failure [35,36] and steatohepatitis [25,37], through inhibiting oxidative stress and inflammation.

Since paeonol has been widely used in clinical applications for treating various types of disease, several paeonol derivatives with considerable drug discovery potential in medicinal chemistry have been synthesized [21]. The introduction of a phenylsulfonyl moiety into a compound was found to improve the solubility of the compound and increase its biological activity [27,28]. Previously, we designed a series of paeonol-phenylsulfonyl derivatives, and showed that 4-MSP significantly inhibits HBV viral gene expression and viral DNA synthesis [29]. Regarding the treatment of liver fibrosis, paeonol has been found to inhibit HSC activation and fibrogenesis [38,39]. In our study, significant antifibrotic effects were observed following treatment with the paeonol-phenylsulfonyl derivative 4-MSP at a lower dosage than that required for paeonol. While Kong et al. reported that 10 μM and 100 mg/kg paeonol could inhibit HSC activation and liver fibrosis, respectively [38], we have shown that 4-MSP inhibits HSC activation and CCl_4-induced liver fibrosis when applied at concentrations of 5 μM and 5 mg/kg, respectively. In addition, 4-MSP-treated mice exhibited no adverse events in terms of body weight loss, hepatotoxicity, or liver dysfunction, suggesting that treatment with 4-MSP is a novel therapeutic option for liver cirrhosis patients. In addition, paeonol administration has been found to prevent other models of fibrosis, such as pulmonary fibrosis and renal fibrosis, via regulating MAPK/Smad, Nrf2/ARE, and Notch1 pathways [40–42]. Except for CCl_4-induced liver fibrosis, the bile duct ligation (BDL) is used to induce obstructive cholestatic injury. BDL promotes the growth of bile duct epithelial cells and portal inflammation, resulting in biliary-type liver fibrogenesis [5]. Activated bile duct epithelial cells synthesize matrix proteins and secret inflammatory mediators (TGF-b, IL-6, MCP1, and PDGF-BB) to activate HSCs. In Figure 5, we showed that 4-MSP expresses its anti-inflammatory potential to inhibit the expression of TNF-α and F4/80. Accordingly, we considered that 4-MSP administration can also attenuate BDL-induced liver damage and fibrosis.

The molecular aims of liver fibrosis therapy are the (1) attenuation of tissue damage and inflammation, (2) inhibition of HSCs' proliferation and activation, (3) induction of HSCs' apoptosis, and (4) promotion of ECM degradation [15,43]. Therefore, it is conceivable that the interference of one of the above steps reduces fibrogenesis. Herein, we explored intracellular pathways that mediate the effects of 4-MSP on HSCs, and focused on PDGF-BB-triggered HSC growth and TGF-β1-induced HSC activation. TGF-β1/Smad pathway is the major signaling involved in the regulation of ECM synthesis, accumulation, and degradation under the progression of liver fibrosis, which further initiates the liver fibrogenesis. Previous studies showed that TGF-β1 is a major factor mediating in the liver fibrosis process of both experimental models and clinical patients with liver diseases [44]. TGF-β1 binds to its receptors and simultaneously phosphorylates the Smad2/3

proteins that further lead to the production of hetero-oligomeric complex with Smad4. Then, this complex is translocated from the cell cytosol into the nuclei of HSCs. This process further induces gene expression of collagen and promotes hepatic fibrosis [45]. Previous studies indicated that mice with Smad3 knockout were protected from the toxicant-induced liver fibrosis [46,47]. TGF-β signaling comprises the C-terminal and linker regions phosphorylation of Smad2 and Smad3 [48]. In Figure 1, we showed that 4-MSP selectively decreases TGF-β1-induced Smad2/3 C-terminal region phosphorylation (p-Smad2(Ser465/467)/p-Smad3(Ser423/425)), α-SMA, and Col1A2 expression. The inhibition of C-terminal phosphorylation is very important for blocking the consequent Smad4 binding and extracellular matrix proteins transcription in the nucleus [48]. The linker region phosphorylation of Smad protein can be regulated by several kinases, such as PI3K/mTORC2, ERK, and JNK [48–52]. In Figure 2, we showed that 4-MSP can decrease the PDGF-BB-induced MEK/ERK, JNK, Akt, and p70S6K phosphorylation. Accordingly, we proposed that 4-MSP may also have the ability to inhibit the phosphorylation of the Smad linker region. Another potent stimulator that regulates HSC proliferation is PDGF-BB. PDGF-BB is able to activate MAPK and Akt signaling during liver fibrogenesis [17]. Moreover, the MAPK/ERK pathway activation is closely correlated with a promotion of cell growth, differentiation, and migration of HSCs [53,54]. In addition, PI3K/Akt and the downstream molecule p70S6K promote cell proliferation, protein synthesis, and collagen gene expression in HSCs [55,56]. Inhibition of either of the MAPK and PI3K/Akt pathways suppressed HSC activation and liver fibrosis [57,58]. Besides this, previous studies showed that PDGF-BB secreted from HSCs would stimulate the HCC cell proliferation through activation of the PI3K/Akt signaling, whereas inhibiting the PDGF-BB or PI3K/Akt signaling would enhance cell apoptosis [59]. In this present study, we have shown that compound 4-MSP has beneficial suppressive effects on both the MAPK and Akt signaling pathways in HSCs treated with PDGF-BB.

5. Conclusions

In summary, we provide experimental evidence to support that 4-MSP selectively suppresses TGF-β1 or/and PDGF-BB-triggered Smad2/3, MAPK, and Akt pathways activation, which are critical for HSCs activation and proliferation (Figure 6). Furthermore, 4-MSP administration significantly ameliorated CCl_4-induced liver fibrosis in mice. In addition, no adverse events in terms of body weight loss, hepatotoxicity, and liver dysfunction were observed in 4-MSP-treated mice. Taken together, these results indicate that 4-methoxy sulfonyl paeonol has significant antifibrotic activity both in vitro and in vivo at a lower dosage than that required for paeonol, which suggests 4-MSP as a novel therapeutic for patients with liver cirrhosis.

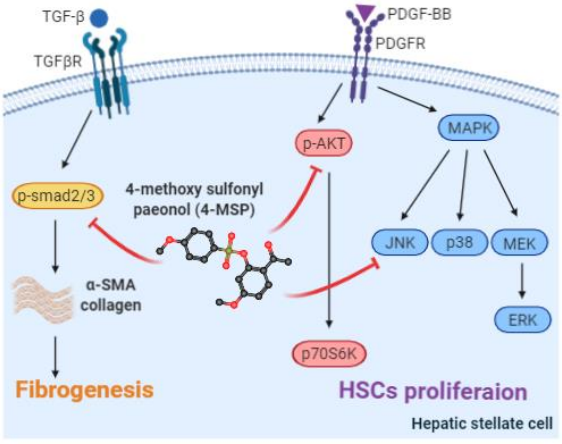

Figure 6. Proposed model of compound 4-methoxy sulfonyl paeonol (4-MSP) in the inhibition of HSCs proliferation and fibrogenesis. Compound 4-MSP causes inhibition of hepatic stellate cells (HSCs) activation and liver fibrosis by blocking TGF-β1/Smad, PDGF-BB/MAPK, and Akt signaling pathways.

Author Contributions: Conceptualization: Y.-J.L., M.-H.H., and F.-M.S.; data curation: Y.-H.W.; formal analysis: Y.-H.W. and C.-C.F.; methodology: C.-L.L.; validation: Y.-J.L. and Y.-H.W.; writing—original draft: Y.-J.L. and Y.-H.W.; writing—review and editing: M.-H.H. and F.-M.S. All authors have read and agreed to the published version of the manuscript.

Funding: This research received no external funding.

Acknowledgments: This work was supported in part by a grant from the Taipei Medical University—Wan Fang Hospital, Taiwan (108-TMU-WFH-10) and from the Ministry of Science and Technology, Taiwan (MOST 109-2628-B-038-020). We also thank Fang-Yu Hsu, Chiao-Fan Liu, Chien-Ying Wu, and Chia-Ying Chien for performing the experiments.

Conflicts of Interest: The authors declare that no competing interests exist with respect to this work.

References

1. Bataller, R.; Brenner, D.A. Liver fibrosis. *J. Clin. Investig.* **2005**, *115*, 209–218. [CrossRef] [PubMed]
2. Schuppan, D.; Afdhal, N.H. Liver cirrhosis. *Lancet* **2008**, *371*, 838–851. [CrossRef]
3. Friedman, S.L. Liver fibrosis—From bench to bedside. *J. Hepatol.* **2003**, *38* (Suppl. 1), S38–S53. [CrossRef]
4. Iredale, J.P.; Thompson, A.; Henderson, N.C. Extracellular matrix degradation in liver fibrosis: Biochemistry and regulation. *Biochim. Biophys Acta* **2013**, *1832*, 876–883. [CrossRef] [PubMed]
5. Iredale, J.P. Models of liver fibrosis: Exploring the dynamic nature of inflammation and repair in a solid organ. *J. Clin. Investig.* **2007**, *117*, 539–548. [CrossRef] [PubMed]
6. Zhang, C.Y.; Yuan, W.G.; He, P.; Lei, J.H.; Wang, C.X. Liver fibrosis and hepatic stellate cells: Etiology, pathological hallmarks and therapeutic targets. *World J. Gastroenterol.* **2016**, *22*, 10512–10522. [CrossRef] [PubMed]
7. Forbes, S.J.; Parola, M. Liver fibrogenic cells. *Best Pract. Res. Clin. Gastroenterol.* **2011**, *25*, 207–217. [CrossRef]
8. Friedman, S.L. Mechanisms of hepatic fibrogenesis. *Gastroenterology* **2008**, *134*, 1655–1669. [CrossRef]
9. Hernandez-Gea, V.; Friedman, S.L. Pathogenesis of liver fibrosis. *Annu. Rev. Pathol.* **2011**, *6*, 425–456. [CrossRef]
10. Friedman, S.L. Hepatic fibrosis—overview. *Toxicology* **2008**, *254*, 120–129. [CrossRef]
11. Lee, U.E.; Friedman, S.L. Mechanisms of hepatic fibrogenesis. *Best Pract. Res. Clin. Gastroenterol.* **2011**, *25*, 195–206. [CrossRef] [PubMed]
12. Majumdar, A.; Curley, S.A.; Wu, X.; Brown, P.; Hwang, J.P.; Shetty, K.; Yao, Z.X.; He, A.R.; Li, S.; Katz, L.; et al. Hepatic stem cells and transforming growth factor beta in hepatocellular carcinoma. *Nat. Rev. Gastroenterol. Hepatol.* **2012**, *9*, 530–538. [CrossRef] [PubMed]
13. Inagaki, Y.; Okazaki, I. Emerging insights into transforming growth factor beta smad signal in hepatic fibrogenesis. *Gut* **2007**, *56*, 284–292. [CrossRef] [PubMed]
14. Schultz, G.S.; Wysocki, A. Interactions between extracellular matrix and growth factors in wound healing. *Wound Repair Regen* **2009**, *17*, 153–162. [CrossRef] [PubMed]
15. Fallowfield, J.A. Therapeutic targets in liver fibrosis. *Am. J. Physiol. Gastrointest. Liver Physiol.* **2011**, *300*, G709–G715. [CrossRef]
16. Yata, Y.; Gotwals, P.; Koteliansky, V.; Rockey, D.C. Dose-dependent inhibition of hepatic fibrosis in mice by a tgf-beta soluble receptor: Implications for antifibrotic therapy. *Hepatology* **2002**, *35*, 1022–1030. [CrossRef]
17. Borkham-Kamphorst, E.; Weiskirchen, R. The pdgf system and its antagonists in liver fibrosis. *Cytokine Growth Factor Rev.* **2016**, *28*, 53–61. [CrossRef]
18. Liu, Y.; Wen, X.M.; Lui, E.L.; Friedman, S.L.; Cui, W.; Ho, N.P.; Li, L.; Ye, T.; Fan, S.T.; Zhang, H. Therapeutic targeting of the pdgf and tgf-beta-signaling pathways in hepatic stellate cells by ptk787/zk22258. *Lab. Investig.* **2009**, *89*, 1152–1160. [CrossRef]
19. He, L.; Tian, D.A.; Li, P.Y.; He, X.X. Mouse models of liver cancer: Progress and recommendations. *Oncotarget* **2015**, *6*, 23306–23322. [CrossRef]
20. Zhang, L.; Li, D.C.; Liu, L.F. Paeonol: Pharmacological effects and mechanisms of action. *Int. Immunopharmacol.* **2019**, *72*, 413–421. [CrossRef]
21. Wang, Z.; He, C.; Peng, Y.; Chen, F.; Xiao, P. Origins, phytochemistry, pharmacology, analytical methods and safety of cortex moutan (paeonia suffruticosa andrew): A systematic review. *Molecules* **2017**, *22*, 946. [CrossRef] [PubMed]

22. Yin, J.; Wu, N.; Zeng, F.; Cheng, C.; Kang, K.; Yang, H. Paeonol induces apoptosis in human ovarian cancer cells. *Acta Histochem.* **2013**, *115*, 835–839. [CrossRef] [PubMed]
23. Lei, Y.; Li, H.X.; Jin, W.S.; Peng, W.R.; Zhang, C.J.; Bu, L.J.; Du, Y.Y.; Ma, T.; Sun, G.P. The radiosensitizing effect of paeonol on lung adenocarcinoma by augmentation of radiation-induced apoptosis and inhibition of the pi3k/akt pathway. *Int. J. Radiat. Biol.* **2013**, *89*, 1079–1086. [CrossRef] [PubMed]
24. Liu, X.; Xu, Q.; Mei, L.; Lei, H.; Wen, Q.; Miao, J.; Huang, H.; Chen, D.; Du, S.; Zhang, S.; et al. Paeonol attenuates acute lung injury by inhibiting hmgb1 in lipopolysaccharide-induced shock rats. *Int. Immunopharmacol.* **2018**, *61*, 169–177. [CrossRef] [PubMed]
25. Hu, S.; Shen, G.; Zhao, W.; Wang, F.; Jiang, X.; Huang, D. Paeonol, the main active principles of paeonia moutan, ameliorates alcoholic steatohepatitis in mice. *J. Ethnopharmacol.* **2010**, *128*, 100–106. [CrossRef]
26. Chen, B.; Ning, M.; Yang, G. Effect of paeonol on antioxidant and immune regulatory activity in hepatocellular carcinoma rats. *Molecules* **2012**, *17*, 4672–4683. [CrossRef]
27. Niwata, S.; Fukami, H.; Sumida, M.; Ito, A.; Kakutani, S.; Saitoh, M.; Suzuki, K.; Imoto, M.; Shibata, H.; Imajo, S.; et al. Substituted 3-(phenylsulfonyl)-1-phenylimidazolidine-2,4-dione derivatives as novel nonpeptide inhibitors of human heart chymase. *J. Med. Chem.* **1997**, *40*, 2156–2163. [CrossRef]
28. Bachovchin, D.A.; Zuhl, A.M.; Speers, A.E.; Wolfe, M.R.; Weerapana, E.; Brown, S.J.; Rosen, H.; Cravatt, B.F. Discovery and optimization of sulfonyl acrylonitriles as selective, covalent inhibitors of protein phosphatase methylesterase-1. *J. Med. Chem.* **2011**, *54*, 5229–5236. [CrossRef]
29. Huang, T.J.; Chuang, H.; Liang, Y.C.; Lin, H.H.; Horng, J.C.; Kuo, Y.C.; Chen, C.W.; Tsai, F.Y.; Yen, S.C.; Chou, S.C.; et al. Design, synthesis, and bioevaluation of paeonol derivatives as potential anti-hbv agents. *Eur. J. Med. Chem.* **2015**, *90*, 428–435. [CrossRef]
30. Twu, Y.C.; Lee, T.S.; Lin, Y.L.; Hsu, S.M.; Wang, Y.H.; Liao, C.Y.; Wang, C.K.; Liang, Y.C.; Liao, Y.J. Niemann-pick type c2 protein mediates hepatic stellate cells activation by regulating free cholesterol accumulation. *Int. J. Mol. Sci.* **2016**, *17*, 1122. [CrossRef]
31. Wang, Y.H.; Suk, F.M.; Liu, C.L.; Chen, T.L.; Twu, Y.C.; Hsu, M.H.; Liao, Y.J. Antifibrotic effects of a barbituric acid derivative on liver fibrosis by blocking the nf-kappab signaling pathway in hepatic stellate cells. *Front. Pharmacol.* **2020**, *11*, 388. [CrossRef] [PubMed]
32. Neff, G.W.; Duncan, C.W.; Schiff, E.R. The current economic burden of cirrhosis. *Gastroenterol. Hepatol.* **2011**, *7*, 661–671.
33. Gressner, O.A.; Weiskirchen, R.; Gressner, A.M. Biomarkers of liver fibrosis: Clinical translation of molecular pathogenesis or based on liver-dependent malfunction tests. *Clin. Chim. Acta* **2007**, *381*, 107–113. [CrossRef] [PubMed]
34. Fan, L.; Song, B.; Sun, G.; Ma, T.; Zhong, F.; Wei, W. Endoplasmic reticulum stress-induced resistance to doxorubicin is reversed by paeonol treatment in human hepatocellular carcinoma cells. *PLoS ONE* **2013**, *8*, e62627. [CrossRef]
35. Ding, Y.; Li, Q.; Xu, Y.; Chen, Y.; Deng, Y.; Zhi, F.; Qian, K. Attenuating oxidative stress by paeonol protected against acetaminophen-induced hepatotoxicity in mice. *PLoS ONE* **2016**, *11*, e0154375. [CrossRef]
36. Gong, X.; Yang, Y.; Huang, L.; Zhang, Q.; Wan, R.Z.; Zhang, P.; Zhang, B. Antioxidation, anti-inflammation and anti-apoptosis by paeonol in lps/d-galn-induced acute liver failure in mice. *Int. Immunopharmacol.* **2017**, *46*, 124–132. [CrossRef]
37. Sun, X.; Wang, P.; Yao, L.P.; Wang, W.; Gao, Y.M.; Zhang, J.; Fu, Y.J. Paeonol alleviated acute alcohol-induced liver injury via sirt1/nrf2/nf-kappab signaling pathway. *Environ. Toxicol. Pharmacol.* **2018**, *60*, 110–117. [CrossRef]
38. Kong, D.; Zhang, F.; Wei, D.; Zhu, X.; Zhang, X.; Chen, L.; Lu, Y.; Zheng, S. Paeonol inhibits hepatic fibrogenesis via disrupting nuclear factor-kappab pathway in activated stellate cells: In vivo and in vitro studies. *J. Gastroenterol. Hepatol.* **2013**, *28*, 1223–1233. [CrossRef]
39. Wu, S.; Liu, L.; Yang, S.; Kuang, G.; Yin, X.; Wang, Y.; Xu, F.; Xiong, L.; Zhang, M.; Wan, J.; et al. Paeonol alleviates ccl4-induced liver fibrosis through suppression of hepatic stellate cells activation via inhibiting the tgf-beta/smad3 signaling. *Immunopharmacol. Immunotoxicol.* **2019**, *41*, 438–445. [CrossRef]
40. Zhang, L.; Chen, Z.; Gong, W.; Zou, Y.; Xu, F.; Chen, L.; Huang, H. Paeonol ameliorates diabetic renal fibrosis through promoting the activation of the nrf2/are pathway via up-regulating sirt1. *Front. Pharmacol.* **2018**, *9*, 512. [CrossRef]

41. Liu, M.H.; Lin, A.H.; Ko, H.K.; Perng, D.W.; Lee, T.S.; Kou, Y.R. Prevention of bleomycin-induced pulmonary inflammation and fibrosis in mice by paeonol. *Front. Physiol.* **2017**, *8*, 193. [CrossRef]
42. Zhou, H.; Qiu, Z.Z.; Yu, Z.H.; Gao, L.; He, J.M.; Zhang, Z.W.; Zheng, J. Paeonol reverses promoting effect of the hotair/mir-124/notch1 axis on renal interstitial fibrosis in a rat model. *J. Cell. Physiol.* **2019**, *234*, 14351–14363. [CrossRef]
43. Friedman, S.L.; Sheppard, D.; Duffield, J.S.; Violette, S. Therapy for fibrotic diseases: Nearing the starting line. *Sci. Transl. Med.* **2013**, *5*, 167sr161. [CrossRef] [PubMed]
44. Leask, A.; Abraham, D.J. Tgf-beta signaling and the fibrotic response. *FASEB J.* **2004**, *18*, 816–827. [CrossRef] [PubMed]
45. Xu, F.; Liu, C.; Zhou, D.; Zhang, L. Tgf-beta/smad pathway and its regulation in hepatic fibrosis. *J. Histochem. Cytochem.* **2016**, *64*, 157–167. [CrossRef]
46. Jeong, D.H.; Hwang, M.; Park, J.K.; Goo, M.J.; Hong, I.H.; Ki, M.R.; Ishigami, A.; Kim, A.Y.; Lee, E.M.; Lee, E.J.; et al. Smad3 deficiency ameliorates hepatic fibrogenesis through the expression of senescence marker protein-30, an antioxidant-related protein. *Int. J. Mol. Sci.* **2013**, *14*, 23700–23710. [CrossRef] [PubMed]
47. Latella, G.; Vetuschi, A.; Sferra, R.; Catitti, V.; D'Angelo, A.; Zanninelli, G.; Flanders, K.C.; Gaudio, E. Targeted disruption of smad3 confers resistance to the development of dimethylnitrosamine-induced hepatic fibrosis in mice. *Liver Int.* **2009**, *29*, 997–1009. [CrossRef] [PubMed]
48. Kamato, D.; Burch, M.L.; Piva, T.J.; Rezaei, H.B.; Rostam, M.A.; Xu, S.; Zheng, W.; Little, P.J.; Osman, N. Transforming growth factor-beta signalling: Role and consequences of smad linker region phosphorylation. *Cell. Signal.* **2013**, *25*, 2017–2024. [CrossRef] [PubMed]
49. Hough, C.; Radu, M.; Dore, J.J. Tgf-beta induced erk phosphorylation of smad linker region regulates smad signaling. *PLoS ONE* **2012**, *7*, e42513. [CrossRef] [PubMed]
50. Yoshida, K.; Matsuzaki, K.; Mori, S.; Tahashi, Y.; Yamagata, H.; Furukawa, F.; Seki, T.; Nishizawa, M.; Fujisawa, J.; Okazaki, K. Transforming growth factor-beta and platelet-derived growth factor signal via c-jun n-terminal kinase-dependent smad2/3 phosphorylation in rat hepatic stellate cells after acute liver injury. *Am. J. Pathol.* **2005**, *166*, 1029–1039. [CrossRef]
51. Kamato, D.; Ta, H.; Afroz, R.; Xu, S.; Osman, N.; Little, P.J. Mechanisms of par-1 mediated kinase receptor transactivation: Smad linker region phosphorylation. *J. Cell Commun. Signal.* **2019**, *13*, 539–548. [CrossRef] [PubMed]
52. Yu, J.S.; Ramasamy, T.S.; Murphy, N.; Holt, M.K.; Czapiewski, R.; Wei, S.K.; Cui, W. Pi3k/mtorc2 regulates tgf-beta/activin signalling by modulating smad2/3 activity via linker phosphorylation. *Nat. Commun.* **2015**, *6*, 7212. [CrossRef] [PubMed]
53. Marra, F.; Arrighi, M.C.; Fazi, M.; Caligiuri, A.; Pinzani, M.; Romanelli, R.G.; Efsen, E.; Laffi, G.; Gentilini, P. Extracellular signal-regulated kinase activation differentially regulates platelet-derived growth factor's actions in hepatic stellate cells, and is induced by in vivo liver injury in the rat. *Hepatology* **1999**, *30*, 951–958. [CrossRef] [PubMed]
54. Wang, Q.; Du, H.; Li, M.; Li, Y.; Liu, S.; Gao, P.; Zhang, X.; Cheng, J. Mapk signal transduction pathway regulation: A novel mechanism of rat hsc-t6 cell apoptosis induced by fuzhenghuayu tablet. *Evid. Based Complementary Altern. Med.* **2013**, *2013*, 368103. [CrossRef]
55. Gabele, E.; Reif, S.; Tsukada, S.; Bataller, R.; Yata, Y.; Morris, T.; Schrum, L.W.; Brenner, D.A.; Rippe, R.A. The role of p70s6k in hepatic stellate cell collagen gene expression and cell proliferation. *J. Biol. Chem.* **2005**, *280*, 13374–13382. [CrossRef]
56. Reif, S.; Lang, A.; Lindquist, J.N.; Yata, Y.; Gabele, E.; Scanga, A.; Brenner, D.A.; Rippe, R.A. The role of focal adhesion kinase-phosphatidylinositol 3-kinase-akt signaling in hepatic stellate cell proliferation and type i collagen expression. *J. Biol. Chem.* **2003**, *278*, 8083–8090. [CrossRef]

57. Son, M.K.; Ryu, Y.L.; Jung, K.H.; Lee, H.; Lee, H.S.; Yan, H.H.; Park, H.J.; Ryu, J.K.; Suh, J.K.; Hong, S.; et al. Hs-173, a novel pi3k inhibitor, attenuates the activation of hepatic stellate cells in liver fibrosis. *Sci. Rep.* **2013**, *3*, 3470. [CrossRef]
58. Peng, Y.; Yang, H.; Wang, N.; Ouyang, Y.; Yi, Y.; Liao, L.; Shen, H.; Hu, G.; Wang, Z.; Tao, L. Fluorofenidone attenuates hepatic fibrosis by suppressing the proliferation and activation of hepatic stellate cells. *Am. J. Physiol. Gastrointest. Liver Physiol.* **2014**, *306*, G253–G263. [CrossRef]
59. Bruix, J.; Boix, L.; Sala, M.; Llovet, J.M. Focus on hepatocellular carcinoma. *Cancer Cell* **2004**, *5*, 215–219. [CrossRef]